AGU PUBLICATIONS

Geophysical Research Letters

RESEARCH LETTER
10.1002/2014GL060559

Key Points:
- Postseismic gravity behaviors of the three M9 earthquakes are very similar
- Postseismic gravity changes are composed of long- and short-term components
- Afterslip and viscoelastic relaxation can be separated by GRACE

Supporting Information:
- Readme
- Figure S1
- Figure S2
- Figure S3
- Figure S4

Correspondence to:
Y. Tanaka,
u39_tanaka@frontier.hokudai.ac.jp

Citation:
Tanaka, Y., and K. Heki (2014), Long- and short-term postseismic gravity changes of megathrust earthquakes from satellite gravimetry, *Geophys. Res. Lett.*, *41*, 5451–5456, doi:10.1002/2014GL060559.

Received 20 MAY 2014
Accepted 5 JUN 2014
Accepted article online 10 JUN 2014
Published online 7 AUG 2014

Long- and short-term postseismic gravity changes of megathrust earthquakes from satellite gravimetry

Yusaku Tanaka[1] and Kosuke Heki[1]

[1]Department of Natural History Sciences, Hokkaido University, Kita-ku, Sapporo, Japan

Abstract Using monthly satellite gravimetry data, we studied time-variable gravity field after three M9 class earthquakes, the 2004 Sumatra-Andaman, 2010 Chile (Maule), and 2011 Tohoku-oki earthquakes. The observations showed that the gravity typically (1) decreases coseismically, (2) continues to decrease for a few months, and (3) increases over a longer period. Therefore, postseismic gravity changes have two components with different time constants and polarities. The mechanisms of short- and long-term postseismic gravity changes are not as clear as coseismic changes at the moment, but might be explained to some extent with afterslip and the Maxwell viscoelasticity, respectively. These two components are difficult to discriminate with surface velocity measurements because the forearc area moves trenchward at both stages. They appear in different polarities in gravity, making satellite gravimetry a unique tool to separate them.

1. Introduction

Theoretical studies predict that earthquakes disturb subsurface mass distributions and change gravity fields (or deform the geoid) [e.g., *Okubo*, 1992]. Such changes were first observed after the 2003 Tokachi-oki earthquake (M_w8.0), Japan, by a ground array of superconducting gravimeters [*Imanishi et al.*, 2004], and after the 2004 Sumatra-Andaman earthquake (M_w9.2) by the Gravity Recovery and Climate Experiment (GRACE) satellites [*Han et al.*, 2006]. GRACE also detected coseismic gravity changes of the 2010 Maule (M_w8.8) [*Heki and Matsuo*, 2010; *Han et al.*, 2010] and the 2011 Tohoku-Oki (M_w9.0) [*Matsuo and Heki*, 2011; *Wang et al.*, 2012a] earthquakes. They showed that coseismic changes are dominated by gravity decrease on the back-arc side (Figure A1) mainly reflecting the density drop of rocks above the downdip end of the fault [*Han et al.*, 2006].

Postseismic gravity changes were found first after the 2004 Sumatra-Andaman earthquake [*Ogawa and Heki*, 2007; *Chen et al.*, 2007]. There postseismic gravity changes are characterized by gravity increases around the ruptured fault (Figure A1) and have been attributed to viscous relaxation of low-viscosity upper mantle rocks [e.g., *Han et al.*, 2008; *Panet et al.*, 2010]. Here we investigate the postseismic gravity changes of all the three M9 class earthquakes mentioned above, using the recent release (RL05) [*Dahle et al.*, 2012; *Chambers and Bonin*, 2012] of the GRACE Level-2 data, and search common features in them.

2. Gravity Data and Time Series Analyses

We used Stokes' coefficients with degrees and orders complete to 60 in the RL05 monthly GRACE data from August 2002 to December 2013 analyzed at the Center for Space Research, University of Texas. In the time series analyses, we used the August 2002 to December 2008 window for the Sumatra-Andaman earthquake, January 2006 to December 2013 for the Maule earthquake, and January 2008 to September 2013 for the Tohoku-Oki earthquake. For the 2004 earthquake, we excluded the data after January 2009 to make its time window of similar length to the other two cases.

To reduce short-wavelength noises, we applied the fan filter with an averaging radius of 250 km [*Zhang et al.*, 2009]. We also reduced longitudinal stripes following *Swenson and Wahr* [2006] using polynomials of degree 3 for coefficients of orders 15 and higher. We had examined two cases, with and without the land hydrology correction by the Global Land Data Assimilation System (GLDAS)/Noah model [*Rodell et al.*, 2004]. We here employed the data without the correction, and only removed average seasonal hydrological contributions by modeling the average annual and semiannual variations in the gravity time series. The Sumatra and NE Japan regions are dominated with sea, and the GLDAS

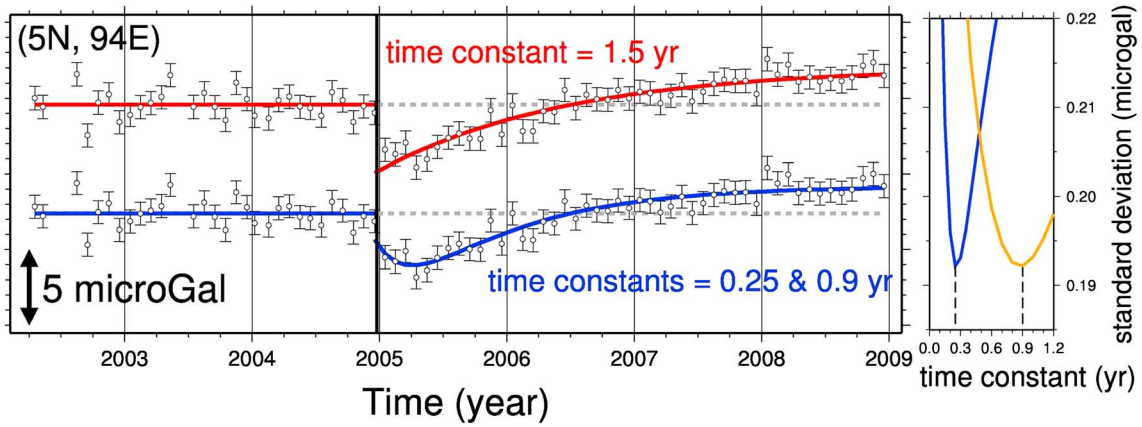

Figure 1. Time series of gravity changes before and after the 2004 Sumatra-Andaman earthquake (black vertical line) at (5N, 94E) fitted with two different models. Average seasonal changes and the secular trend are removed. With the red and blue curves, the postseismic changes are modeled with one (τ: 1.5 years) and two exponential decay functions (τ_1: 0.25 years and τ_2: 0.90 years), respectively. The right figure shows the sensitivity of the standard deviation of the gravity data residuals 2005.0–2005.5 to the changes of one of the time constants (blue: τ_1, yellow: τ_2) for the two-function model. The data and the blue curve appear again and are compared with other events in Figure 3.

corrections do not yield significant differences. In the Chilean case, fairly large hydrological signals were seen in the continental region to the east, but GLDAS did not effectively reduce them. There was a severe drought in South America in 2010 [e.g., *Lewis et al.*, 2011], and this may not be well modeled in GLDAS. In the supporting information (Figure A2), we give the time series with GLDAS corrections for the three cases to show that the overall story is not affected by hydrological noises.

Figure 1 shows the gravity time series at a point just above the fault of the 2004 Sumatra-Andaman earthquake (black circle in Figure 2a). Average seasonal changes and linear trends were removed. Here, the time series was modeled with equation (1). The postseismic gravity changes (Δg) are modeled with the combination of two exponential functions with different time constants, i.e.,

$$\Delta g = A + Bt + C\sin(\omega t + \theta_1) + D\sin(2\omega t + \theta_2) + H(\Delta t)\left[E + F_1\left\{1 - \exp\left(\frac{-\Delta t}{\tau_1}\right)\right\} + F_2\left\{1 - \exp\left(\frac{-\Delta t}{\tau_2}\right)\right\}\right], \quad (1)$$

where A is the offset, B is the average linear trend, and the seasonal changes are expressed with the third and the fourth terms. The constant ω denotes the angular velocity of the annual sinusoid, and C, D, θ_1, and θ_2 denote amplitudes and initial phases of annual and semi-annual components. Δt is the time from the earthquake occurrence. The step function $H(\Delta t)$ is 0 and 1 for negative and positive Δt, respectively. The coseismic gravity step is expressed with E, and the F_1 and F_2 are the coefficients of the postseismic changes with time constants τ_1 and τ_2, respectively.

In Figure 1, the time series was modeled in two different ways. First (red curve), we modeled the postseismic change with a single exponential decay function (i.e., F_1 is fixed to zero). We fixed the time constant τ_2 to 1.5 years, and estimated the eight parameters A, B, $C\cos\theta_1$, $C\sin\theta_1$, $D\cos\theta_2$, $D\sin\theta_2$, E, and F_2 with the least squares method. The data show slight misfit from the model at the early postseismic stage, i.e., gravity keeps decreasing for a few months immediately after the earthquake.

Second (blue curve), we considered two exponential decay functions, and added F_1 as a parameter to be estimated. We tested various values for the time constants τ_1 and τ_2, and found that $\tau_1 = 0.25$ (years) and $\tau_2 = 0.90$ (years) minimize the post-fit residuals of the gravity data (Figure 1 right). The shorter time constant ($\tau_1 = 0.25$ years) fits well (and the longer time constant τ_2 does not) with the eastward movement of the Global Navigation Satellite System (GNSS) station at SAMP in North Sumatra (Figure 4a) for the 3 months postseismic period (the 2005 Nias earthquake occurred ~3 months after the Sumatra-Andaman event and disrupted the time series). Figure A3 shows the sensitivity of the results to different values of τ_1.

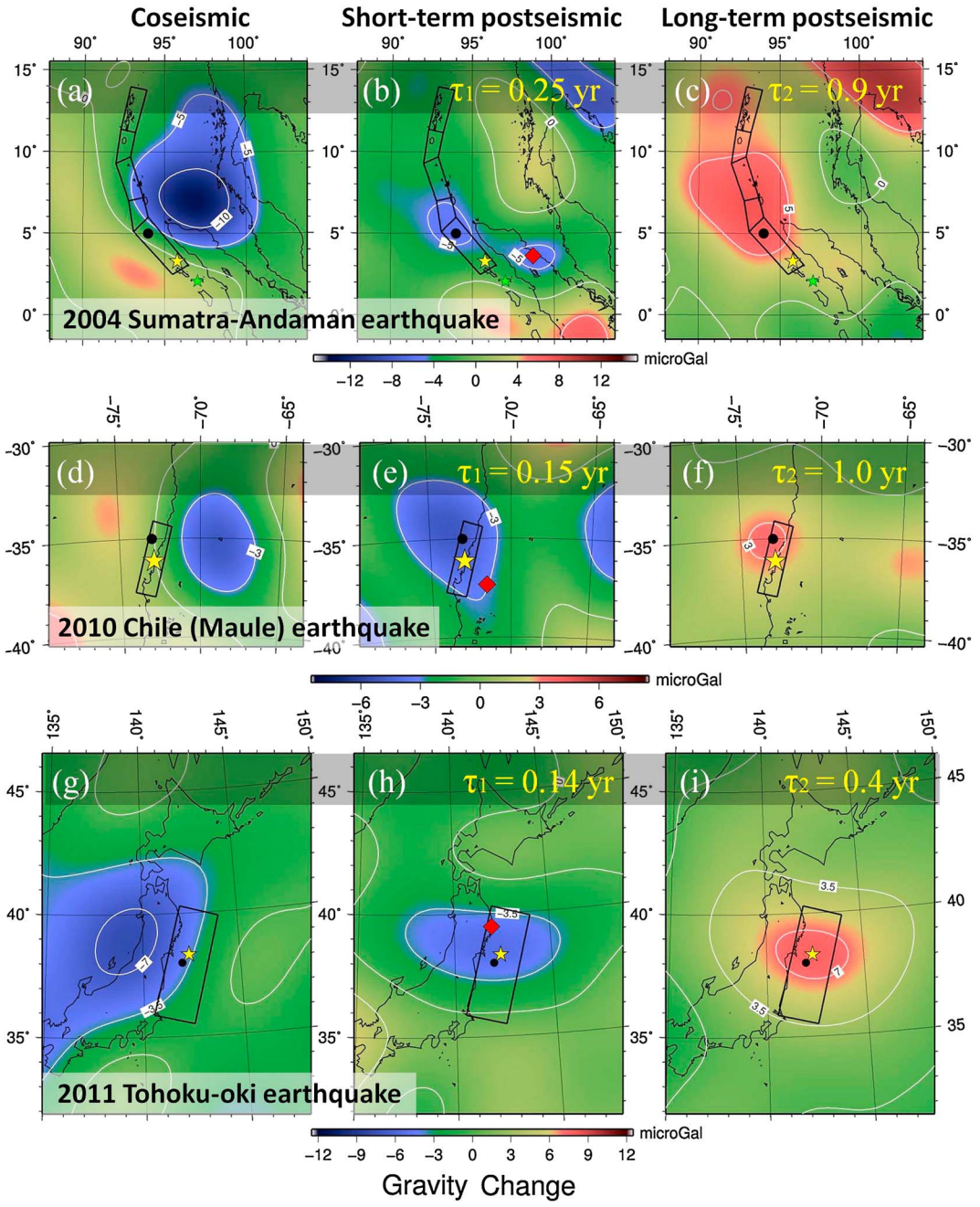

Figure 2. (Left) Coseismic, and (middle) short- and (right) long-term postseismic gravity changes (expressed with 1 year cumulative changes) of the 2004 Sumatra-Andaman (high), the 2010 Maule (middle), and the 2011 Tohoku-oki (low) earthquakes. Time constants for the postseismic changes are shown on the middle and right columns. The yellow stars and black rectangles show the epicenters and the ruptured faults. The black circles show points whose gravity changes are shown in Figures 1 and 3, and red diamonds in the middle column show Global Navigation Satellite System (GNSS) stations shown in Figure 4. The contour intervals in high, middle, and low rows are 5, 3, and 3.5 μGal, respectively.

At each of the grid points with 1 degree separation, we modeled the time series of the GRACE data using equation (1). We used the same values for τ_1 and τ_2, and estimated the same set of parameters. The average post-fit residual of the gravity was ~0.5 μGal. The residuals tend to be larger/smaller at grid points within land/sea, but remain within 0.4–0.7 μGal at most of the points. The geographical distributions of the estimated parameters E, F_1, and F_2 are shown in Figures 2a–2c (F_1 and F_2 are scaled so that they show 1 year cumulative changes).

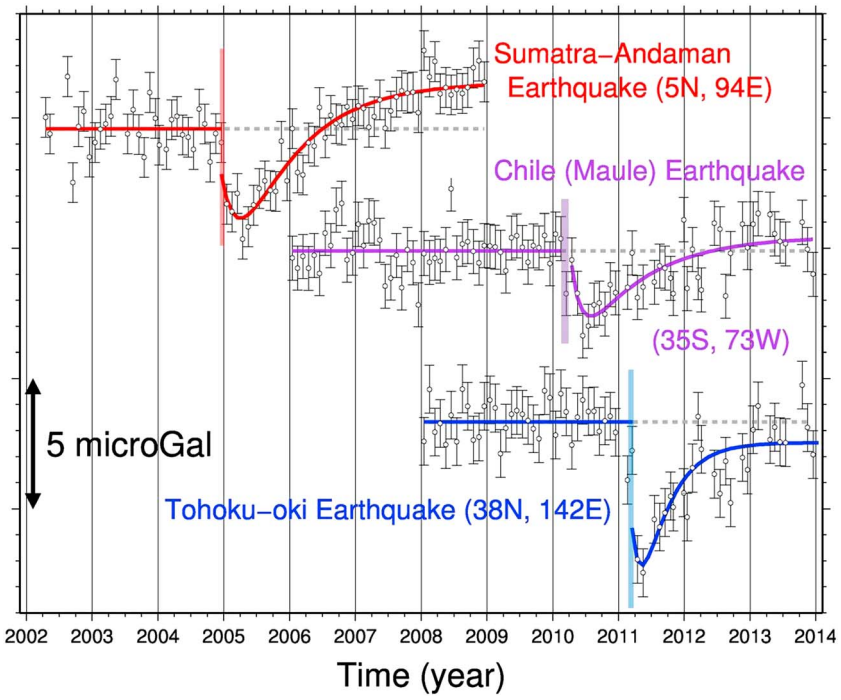

Figure 3. Time series of gravity changes before and after the three megathrusts (colored vertical lines) at points close to the epicenters (black circles in Figure 2). Errors are assumed uniform in time and have been scaled using post-fit residuals (0.5–0.6 μGal in this figure). Land hydrology corrections are not performed, but the average seasonal changes and secular trends are removed. All the three cases suggest the existence of two postseismic gravity change components with distinct time constants and polarities. The transition from decrease to increase is quicker in the Tohoku-oki case than the other two because the time constant of its long-term component is relatively short (0.4 years).

The time series for the 2010 and 2011 cases were also modeled with equation (1) and shown in Figure 3. For these two earthquakes, it was difficult to constrain the shorter time constants in this way (residuals did not show clear minima like in the 2004 earthquake). Instead, we assumed that the short-term postseismic gravity changes in these two earthquakes obey the same exponential decay as surface displacements, and gave time constants (0.15 and 0.14 years) that best fit the GNSS data during the first four postseismic months (Figures 4b and 4c). In such a short timescale, Maxwellian viscous relaxation would contribute little, and

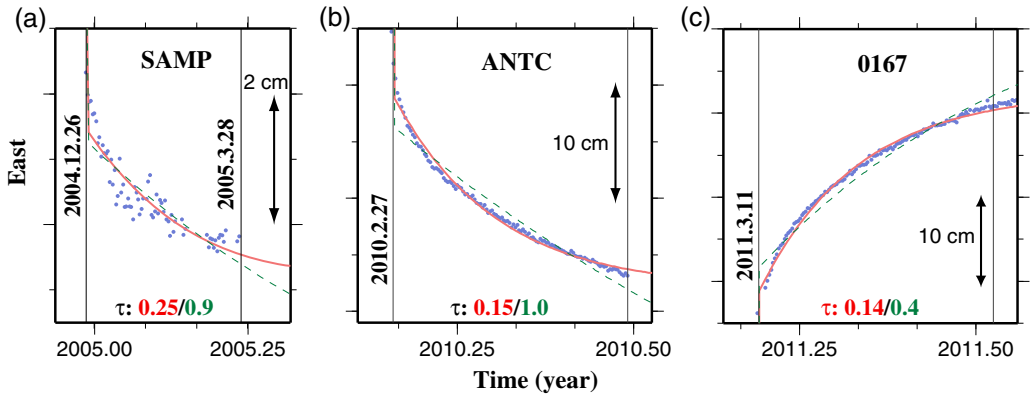

Figure 4. East components of the movements of the GNSS stations (SAMP, ANTC, and 0167 shown in Figures 2b, 2e, and 2h) showing postseismic crustal movements over 3–4 months after the three megathrust events. The data are from http://sideshow.jpl.nasa.gov/post/series.html (SAMP and ANTC) and http://mekira.gsi.go.jp (0167). The solid (red) and dashed (blue) curves are the best-fit exponential decay functions with the time constants of the short- and long-term postseismic gravity changes (shown at the bottom), respectively.

afterslips would be mainly responsible for these changes. Figures 2d–2h show the distribution of E, F_1, and F_2 for these two events. The values of τ_1 and τ_2 are shown in the middle and right columns of Figure 2.

3. Results and Discussion

3.1. Coseismic Gravity Changes

Figure 2 compares the distribution of coseismic, and short- and long-term postseismic gravity changes of the three megathrust events. Although their signal-to-noise ratio is sometimes low, common gravity change signatures are seen. Coseismic signatures of the three earthquakes (Figures 2a, 2d, and 2g) are dominated by gravity decreases on the upper-plate side of the fault, mainly in the back arc area, with smaller increases on the incoming-plate side. The latter are often attenuated by the existence of seawater [*Heki and Matsuo*, 2010; *Matsuo and Heki*, 2011].

Such coseismic changes are well understood as the response of the elastic and stratified Earth to fault slip, i.e., vertical deformation of layer boundaries with density contrasts (such as Moho and the surface) and changes in density associated with the volumetric strain of rocks. The signature of the density change becomes predominant after spatial filtering [*Han et al.*, 2006]. The dominance of the negative change is understood as the manifestation of downward mass transports (subduction) realized as density changes (rocks above/below the downdip end of the fault become lighter/denser) caused by fault slip (Figure A1).

3.2. Short-Term Postseismic Gravity Changes

Figure 3 shows that the gravity decreases as the continuation of the coseismic step for a few months and increases over longer periods. The short-term postseismic gravity changes (Figures 2b, 2e, and 2h) are largely negative and similar to coseismic changes (Figures 2a, 2d, and 2g), although their maxima seem to shift somewhat trenchward. On the other hand, the long-term postseismic gravity changes (Figures 2c, 2f, and 2i) are mostly positive with their maxima residing roughly on the ruptured faults. These features are common in the three earthquakes.

The elastic response to the afterslip should occur as the continuation of the coseismic gravity changes, and their spatial distribution should show some similarity. The time constants (0.14–0.25 years) in the displacement of GNSS stations over the first few postseismic months are consistent with such short-term negative changes, and not with the long-term positive changes (Figure 4). These similarities in temporal signatures strongly indicate that the short-term gravity changes are due to afterslips (delayed elasticity by the transient rheology [*Wang et al.*, 2012b] may contribute to some extent). Afterslip occurs both updip and downdip of the coseismic rupture zone. The trenchward shifts of the centers of the short-term postseismic gravity decreases might reflect the sensitivity contrast, i.e., shallower slips make larger gravity signals. The short-term gravity change of the Maule earthquake is almost as large as the coseismic change, although the other two earthquakes do not show such peculiarity. This might suggest the role of transient viscoelastic relaxation but needs future studies.

It should be noted here that the short-term postseismic change of the 2004 Sumatra-Andaman earthquake (Figure 2b) might include the signal of the coseismic gravity steps of the 2005 March 28 Nias earthquake (M_w8.6), as shown by a small negative anomaly around (99W 6S).

3.3. Long-Term Postseismic Gravity Changes

The Maxwell viscoelasticity explains the slow convergent movements of lithosphere in subduction zones over years to decades after megathrust earthquakes (see Figure 2 of *Wang et al.* [2012a]). Such a movement would promote gravity increase around the ruptured fault (Figure A1).

The "long-term" postseismic gravity change of the 2004 Sumatra-Andaman earthquake has been explained by such viscous relaxation of the upper mantle [e.g., *Han et al.*, 2008; *Panet et al.*, 2010]. Indeed, the cumulative gravity changes over the two postseismic years (Figure A4) calculated assuming a spherically symmetric viscoelastic Earth model [*Tanaka et al.*, 2006, 2007, and *Tanaka*, 2013] show a striking similarity to Figure 2c, suggesting its strong potential to explain long-term postseismic gravity changes. However, in order to match the calculation with the observation, we have to assume the upper mantle viscosity (e.g., Figure A4 assumes 3×10^{18} Pa s) lower by two orders of magnitude than the global average of 10^{20}–10^{21} Pa s [*Moucha et al.*, 2007]. In this context, the upward diffusion of supercritical water around the downdip end of the ruptured fault, as suggested by *Ogawa and Heki* [2007], could help explain some parts of the postseismic gravity recoveries that are too fast to be due to the Maxwell viscoelasticity.

In the top two cases in Figure 3, the long-term gravity increases are more than the short-term drops causing net gravity increase just above the faults. However, gravity shows net decrease in the back-arc side of trenches. A long-term balance of gravity changes in a whole earthquake cycle is an interesting issue. However, quantitative discussion is premature at the moment because satellite gravimetry has not succeeded in detecting slow gravity changes associated with interseismic strain buildup yet.

4. Conclusions

We studied postseismic gravity changes following three M9 class earthquakes and found that they had two components, i.e., short- and long-term gravity changes. The coseismic gravity decrease is followed by continuing decrease in the first few months, and then a gradual increase over years. The physical mechanisms of the short- and long-term postseismic gravity changes would be explained with afterslip (and partly by the transient rheology) and relaxation of Maxwell viscoelastic material (and partly by the movement of supercritical water at depth).

GNSS networks are deployed in many convergent plate boundaries. However, they are on the island/continental arcs with a certain distance from trenches. As shown in *Wang et al.* [2012b], both afterslip and viscoelastic relaxation cause trenchward movements there, and it is difficult for GNSS receivers to observe the transition from the former to the latter. The satellite gravimetry offers a new sensor to investigate deformation cycles of subduction earthquakes in a unique approach different from conventional sensors (Figure A1).

Acknowledgments
We thank Koji Matsuo (Kyoto University) for discussions and Yoshiyuki Tanaka (University of Tokyo) for Figure A4, and two anonymous reviewers for constructive comments. Data can be downloaded from following URLs, GRACE: ftp://podaac.jpl.nasa.gov/allData/grace/L2/CSR/RL05, GEONET: http://mekira.gsi.go.jp, GNSS (JPL): http://sideshow.jpl.nasa.gov/post/series.html, and GLDAS: http://disc.sci.gsfc.nasa.gov/. The data needed to make Figure A4 will be available on request (contact to u39_tanaka@frontier.hokudai.ac.jp).

The Editor thanks two anonymous reviewers for their assistance in evaluating this paper.

References

Chambers, D., and J. A. Bonin (2012), Evaluation of Release-05 GRACE time-variable gravity coefficients over the Ocean, *Ocean Sci. Discuss.*, *9*, 2187–2214, doi:10.5194/osd-9-2187-2012.

Chen, J. L., C. R. Wilson, B. D. Tapley, and S. Grand (2007), GRACE detects coseismic and postseismic deformation from the Sumatra-Andaman earthquake, *Geophys. Res. Lett.*, *34*, L13302, doi:10.1029/2007GL030356.

Dahle, C., F. Flechtner, C. Gruber, D. König, R. König, G. Michalak, and K.-H. Neumayer (2012), GFZ GRACE Level-2 processing standards document for level-2 product release 0005, *Sci. Tech. Rep. GFZ Potsdam*, 20 pp., Germany, doi:10.2312/GFZ.b103-12020.

Han, S.-C., C. K. Shum, M. Bevis, C. Ji, and C.-Y. Kuo (2006), Crustal dilatation observed by GRACE after the 2004 Sumatra-Andaman earthquake, *Science*, *313*, 658–662, doi:10.1126/science.1128661.

Han, S.-C., J. Sauber, S. B. Luthcke, C. Ji, and F. F. Pollitz (2008), Implications of postseismic gravity change following the great 2004 Sumatra-Andaman earthquake from the regional harmonic analysis of GRACE intersatellite tracking data, *J. Geophys. Res.*, *113*, B11413, doi:10.1029/2008JB005705.

Han, S.-C., J. Sauber, and S. Luthcke (2010), Regional gravity decrease after the 2010 Maule (Chile) earthquake indicates large-scale mass redistribution, *Geophys. Res. Lett.*, *37*, L23307, doi:10.1029/2010GL045449.

Heki, K., and K. Matsuo (2010), Coseismic gravity changes of the 2010 earthquake in central Chile from satellite gravimetry, *Geophys. Res. Lett.*, *37*, L24306, doi:10.1029/2010GL045335.

Imanishi, Y., T. Sato, T. Higashi, W. Sun, and S. Okubo (2004), A network of superconducting gravimeters detects submicrogal coseismic gravity changes, *Science*, *306*, 476–478, doi:10.1126/science.1101875.

Lewis, S. L., P. M. Brando, O. L. Phillips, G. M. F. van der Heijden, and D. Nepstad (2011), The 2010 Amazon drought, *Science*, *331*, 554, doi:10.1126/science.1200807.

Matsuo, K., and K. Heki (2011), Coseismic gravity changes of the 2011 Tohoku-Oki earthquake from satellite gravimetry, *Geophys. Res. Lett.*, *38*, L00G12, doi:10.1029/2011GL049018.

Moucha, R., A. Forte, J. X. Mitrovica, and A. Daradich (2007), Lateral variations in mantle rheology: Implications for convention related surface observables and inferred viscosity models, *Geophys. J. Int.*, *169*, 113–135, doi:10.1111/j.1365-246X.2006.03225.x.

Ogawa, R., and K. Heki (2007), Slow postseismic recovery of geoid depression formed by the 2004 Sumatra-Andaman earthquake by mantle water diffusion, *Geophys. Res. Lett.*, *34*, L06313, doi:10.1029/2007GL029340.

Okubo, S. (1992), Gravity and potential changes due to shear and tensile faults in a half-space, *J. Geophys. Res.*, *97*, 7137–7144.

Panet, I., F. Pollitz, V. Mikhailov, M. Diament, P. Banerjee, and K. Grijalva (2010), Upper mantle rheology from GRACE and GPS postseismic deformation after the 2004 Sumatra-Andaman earthquake, *Geochem. Geophys. Geosyst.*, *11*, Q06008, doi:10.1029/2009GC002905.

Rodell, M., et al. (2004), The Global Land Data Assimilation System, *Bull. Am. Meteorol. Soc.*, *85*, 381–394, doi:10.1175/BAMS-85-3-381.

Swenson, S. C., and J. Wahr (2006), Post-processing removal of correlated errors in GRACE data, *Geophys. Res. Lett.*, *33*, L08402, doi:10.1029/2005GL025285.

Tanaka, Y. (2013), Theoretical computation of long-term postseismic relaxation due to a great earthquake using a spherically symmetric viscoelastic Earth model [in Japanese], *J. Geod. Soc. Jpn.*, *59*, 1–10.

Tanaka, Y., J. Okuno, and S. Okubo (2006), A new method for the computation of global viscoelastic post-seismic deformation in a realistic earth model (I)-vertical displacement and gravity variation, *Geophys. J. Int.*, *164*, 273–289, doi:10.1111/j.1365-246X.2005.02821.x.

Tanaka, Y., J. Okuno, and S. Okubo (2007), A new method for the computation of global viscoelastic post-seismic deformation in a realistic earth model (II)-horizontal displacement, *Geophys. J. Int.*, *170*, 1031–1052, doi:10.1111/j.1365-246X.2007.03486.x.

Wang, L., C. K. Shum, F. J. Simons, B. Tapley, and C. Dai (2012a), Coseismic and postseismic deformation of the 2011 Tohoku-Oki earthquake constrained by GRACE gravimetry, *Geophys. Res. Lett.*, *39*, L07301, doi:10.1029/2012GL051104.

Wang, K., Y. Hu, and J. He (2012b), Deformation cycles of subduction earthquakes in a viscoelastic Earth, *Nature*, *484*, 327–332, doi:10.1038/nature11032.

Zhang, Z.-Z., B. F. Chao, Y. Lu, and H.-T. Hsu (2009), An effective filtering for GRACE time-variable gravity: Fan filter, *Geophys. Res. Lett.*, *36*, L17311, doi:10.1029/2009GL039459.